Nulling Performance on Antenna Patterns Using Multiple Null Constraints Vs. Derivative Constraints

by

Tony V. Maesto

B.S.E.E., University of Massachusetts at Lowell (1996)

Submitted to the Department of Electrical Engineering and Computer Science
in partial fulfillment of the requirements for the degree of

Master of Science in Electrical Engineering and Computer Science

at the

MASSACHUSETTS INSTITUTE OF TECHNOLOGY

June 1999

Author .....
Department of Electrical Engineering and Computer Science
May 07, 1999

Certified by .....
Arthur B. Baggeroer
Professor of Electrical and Ocean Engineering
Thesis Supervisor

Accepted by .....
Arthur C. Smith
Chairman, Departmental Committee on Graduate Students

Nulling Performance on Antenna Patterns Using Multiple Null Constraints Vs. Derivative Constraints

by

Tony V. Maesto

Submitted to the Department of Electrical Engineering and Computer Science
on May 07, 1999, in partial fulfillment of the
requirements for the degree of
Master of Science in Electrical Engineering and Computer Science

Abstract

A comparison study on the performance of two antenna pattern nulling techniques is being investigated. The two nulling techniques are Multiple Null Constraints and Derivative Constraints. The method of Multiple Null Constraints technique consists of placing a set of closely spaced single nulls over a desired nulling sector, while Derivative Constraints technique consists of placing a single null at the center of the nulling sector and simultaneously imposing zero derivative(s) response at the same point. For a given number of constraints imposed on the pattern to obtain a desire pattern null characteristic, the amount of null depth and null width achieved and the pattern white noise gain will be compared under each nulling technique.

Thesis Supervisor: Arthur B. Baggeroer
Title: Professor of Electrical and Ocean Engineering

Acknowledgments

I like to thank my thesis advisor Arthur B. Baggeroer for his technical guidance. Thanks to those who have helped me in so many ways during my time at MIT. Thanks to the Staff and all the members of the Ocean Engineering Acoustics Group for all their help. Thanks to Vincent for proof reading this thesis.

I would like to thank Raytheon for its financial support via the Miccioli Fellowship Program. Thanks to Chibl Nahas and Dave Blackstone at Raytheon for their support in the fellowship application process.

I would like to especially thank Mrs. Constance Driscoll for her continuing support in my academic endeavor.

From the bottom of my heart, I want to express my deepest appreciation to my family, my Dad and my Sister which have been a constant source of encouragement to me through their love and their prayers. Above all, I acknowledge that all my success comes from God who has been my strength and my hope.

Contents

List of Figures

Chapter 1

Introduction

Antenna pattern nulling is a method used to suppress interference in the beam pattern by means of placing nulls in the directions of the interfering sources. Null placement in beam patterns has found applications in radar and sonar systems as an effort to minimize the degradation in the signal-to-noise ratio.

1.1 The Problem

A narrow-band interference signal can be suppressed by placing a null or by constraining the beam pattern to have zero gain in the interfering direction. However, a broad null is required to null over a finite angular sector when the interfering signal is spatially wide-band and when the direction of arrival of the unwanted signal varies slightly with time or is not known exactly. A number of techniques have been published in the area of antenna pattern synthesis to obtain broader pattern nulls [1]-[3].

Multiple Null Constraints is a technique often used to obtain broader pattern nulls [2], [3]. The technique imposes constraints on the beam pattern by placing a set of closely spaced single nulls over the desired angular sector. In antenna pattern synthesis problems, we are generally given a beam pattern and are asked to obtain a synthesized pattern which is similar to the original pattern but is subjected to some pattern constraints. In our problem of interest, the pattern constraints are nulls. This

generally involves finding a *constrained* weight vector that is an approximate of the original weight vector.

1.2 The Goal

The objective here is to obtain a constrained pattern with good null responses in the interfering directions while minimizing changes to the original pattern in directions away from the constraint points (especially inside the mainlobe) . There were no criteria to minimize changes in the pattern in previous works [2] and [3]. As an improvement to these efforts, part of this thesis develops a modified Multiple Null Constraints technique using a least mean squared error criteria for changes in the pattern.

1.3 New Approach

Alternatively, broader nulls can also be achieved by constraining a zero-order null together with higher order derivative nulls at the null location [4]. Zero-order pattern nulling is the same as the method of Multiple Null Constraints using a single null. The broader null width is the result of the constraint that the higher order derivatives are zero at the null location. Constraining zero derivative gain at a null location forces little changes in the vicinity of the null point. Thus, a flatter or wider null is achieved. This beam pattern nulling technique is called Derivative Constraints and its results will be presented in a later chapter.

Two pattern nulling techniques, Multiple Null Constraints and Derivative Constraints, will be studied and their results will be compared via a Least-Mean-Square pattern synthesis technique which will be developed in this thesis.

The performance of each nulling technique is evaluated based on its ability to achieve the broadest possible null width and depth and the array white noise gain for a given number of constraints imposed on the beam pattern.

Chapter 2

Background

2.1 Multiple Null Constraints

Various antenna pattern nulling techniques have been published over the years in trying to suppress interference from certain directions in the antenna beam pattern [1]-[3]. Davies [1] described a method employing a network of phase shifters for independent control of the angular location of the zeros in the beam pattern. This technique was derived by expressing the directional pattern of the N-element linear array in a polynomial form of order N-1, and representing it as the product of N-1 factors thus giving N-1 zeros of the directional pattern. A sector null can be formed if several nulls are made to lie within a desired angular sector.

The technique proposed by Drane-McIlvenna [2] maximizes the array gain in some prespecified direction while placing pattern nulls in the direction of the interference. The authors took advantage of the special properties of the constraint matrix and derived an eigenvector solution for the amplitude and phase of the optimal array excitation coefficients.

Another multiple null constraints method was solved adaptively by Applebaum [3]. In the presence of interference, the pattern adaptively places nulls in the direction of the interference thus maximizing the signal-to-noise ratio. This is done by forming a cancellation beam pattern and subtracting it from the normal or *quiescent* beam pattern. The cancellation pattern has the same shape as the quiescent pattern except

that it is centered at the interfering direction and appropriately scaled.

One unattractive feature of the above null placement techniques is the lack of control in the change of the pattern's shape away from the constraint points. Higher sidelobe levels or an undesirable shape can occur due to the absence of criteria on the difference between the constrained and the quiescent patterns away from the constrained points. Ideally one would like to preserve the main beam's response while constraining the pattern to have some desired null response.

2.2 Derivative Constraints

In the past, derivative constraint techniques have been used to broaden the beamwidth in the look direction of a beam pattern to avoid accidental signal suppression [4], [5]. This is done by controlling the first few derivatives of the pattern function at the points of interest. Specifically, the derivative(s) of the pattern are constrained to have zero gain at the points of interest. Imposing a zero derivative gain at a point minimizes rapid changes in the pattern in the vicinity of that point. Thus, the beamwidth can be made flatter or broader when higher order derivative patterns are added to the zeroth order pattern.

In this work, the author is proposing a technique that uses derivative constraints to obtain broader pattern nulls instead of a broader beamwidth as it was used in [4] and [5]. A least mean square pattern change criteria will be imposed to assure minimal changes away from the constrained points.

Chapter 3

Problem Formulation

3.1 Methodology

For a linear array of N+1 isotropic antenna elements with uniform spacing, the antenna farfield wavenumber response function is given by

$$W(\underline{k}) = \sum_{n=-N/2}^{N/2} w_n e^{-j\underline{k}\cdot\underline{z}_n}, \tag{3.1}$$

where $\underline{k}$ is the spatial wavenumber vector, w_n is the weighting coefficient for the nth array element and $\underline{z}_n$ is the relative spatial location for the nth element. For the line array shown in Figure 3-1, the spatial location of each element reduces to

$$\underline{z}_n = nd\underline{a}_x, \tag{3.2}$$

where d is the interelement spacing and $\underline{a}_x$ is the unit vector along the x-direction.

The *quiescent* or normal wavenumber response function is defined as

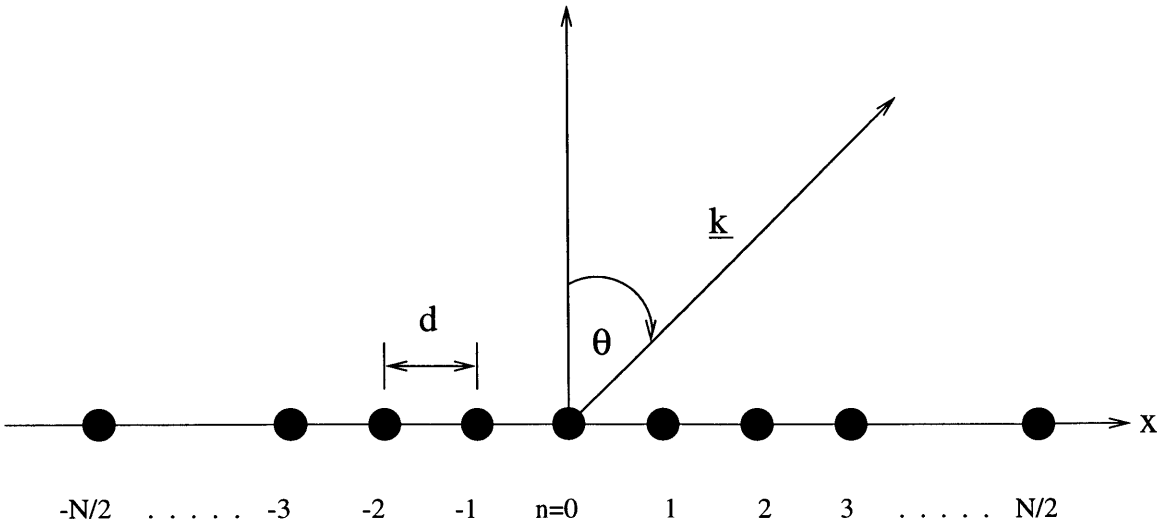

Figure 3-1: Line Array (The dots represents array elements)

$$W_q(k_x) = \sum_{n=-N/2}^{N/2} q_n e^{-jndk_x}, \tag{3.3}$$

where q_n is the individual array element weight coefficient and k_x is the x-component of the spatial wavenumber given by

$$k_x = \frac{2\pi}{\lambda} \sin(\theta), \tag{3.4}$$

where λ is the wavelength and θ is the observation angle measured from the broadside direction.

Similarly, the *constrained* wavenumber response function W_c is defined as

$$W_c(k_x) = \sum_{n=-N/2}^{N/2} c_n e^{-jndk_x}, \tag{3.5}$$

where c_n is the weighting coefficient for the nth array element. This constrained function W_c is an approximation of the quiescent function W_q subjected to either

Multiple Null Constraints or Derivative Constraints.

Our objective is to find a constrained wavenumber response function W_c which is a least mean squared error approximation of the quiescent wavenumber response function W_q subject to Multiple Null Constraints or Derivative Constraints. By examining (3.3) and (3.5), we see that the shape of a wavenumber response function is characterized by its array weighting coefficients. Therefore, the posed problem is to find a set of excitation coefficients c_n, such that the resulting pattern W_c is the least mean squared error approximation of the quiescent pattern W_q.

3.1.1 Mean Squared Error

The mean squared difference between the quiescent and the constrained wavenumber response functions, Eqns. (3.3) and (3.5), is

$$\epsilon = \frac{\lambda}{4\pi} \int_{-2\pi/\lambda}^{2\pi/\lambda} |W_q(k_x) - W_c(k_x)|^2 dk_x. \tag{3.6}$$

Substituting (3.3) and (3.5) into (3.6) yields

$$\epsilon = \frac{\lambda}{4\pi} \int_{-2\pi/\lambda}^{2\pi/\lambda} \left| \sum_{n=-N/2}^{N/2} e^{-jndk_x} (q_n - c_n) \right|^2 dk_x. \tag{3.7}$$

In the special case of an interelement spacing of one-half of a wavelength, $d = \lambda/2$, the mean squared error reduces to

$$\epsilon = \sum_{n=-N/2}^{N/2} |q_n - c_n|^2 \tag{3.8}$$

after integrating equation (3.7). The results shown in (3.8) indicate that the mean squared error between two patterns is completely characterized by their excitation

coefficients. This is expected since the shape of the wavenumber response function is determined by the excitation coefficients.

Alternatively, the mean squared error can be expressed in vector form as

$$\epsilon = \left\| \underline{q} - \underline{c} \right\|^2, \tag{3.9}$$

where $\underline{q}$ and $\underline{c}$ are the array weighting vectors for the quiescent and the constrained patterns, respectively. They are defined as:

$$\underline{q} = [q_{-\frac{N}{2}}, \ldots, q_0, \ldots, q_{\frac{N}{2}}], \tag{3.10}$$

and

$$\underline{c} = [c_{-\frac{N}{2}}, \ldots, c_0, \ldots, c_{\frac{N}{2}}], \tag{3.11}$$

respectively. In vector form, the mean squared error between two patterns is the squared norm of the difference in their corresponding weight vectors.

3.1.2 Multiple Null and Derivative Constraints

Utilizing the mean squared error between the quiescent and the constrained patterns expressed in (3.9), the pattern approximation can now be stated as follows:

$$\text{Arg}\min_{\underline{c}} \epsilon = \left\| \underline{q} - \underline{c} \right\|^2, \tag{3.12}$$

$$\text{subject to } \frac{\partial^i}{\partial k_x^i} W_c(k_{x\alpha}) = 0, \tag{3.13}$$

where $i = 0, ..., N_1 - 1$, is the order of the derivative and $\alpha = 1, ..., N_2$, is the null wavenumber location. In view of (3.13), the constrained wavenumber response function is subjected to Multiple Null Constraints when $i = 0$ and is subjected to Derivative Constraints when $i \geq 1$.

The i^{th} order derivative of the constrained wavenumber response function, Eq. (3.5), at a particular null location is

$$\frac{\partial^i}{\partial k_x^i} W_c(k_{x\alpha}) = \sum_{n=-N/2}^{N/2} c_n (-jnd)^i e^{-jndk_{x\alpha}} = 0. \tag{3.14}$$

From (3.14), we now define the constraint vector for each null constraint as

$$\underline{E}(k_{x\alpha}) = [(j\frac{N}{2}d)^i e^{j\frac{N}{2}dk_{x\alpha}}, \ldots, 1, \ldots, (-j\frac{N}{2}d)^i e^{-j\frac{N}{2}dk_{x\alpha}}]^*, \tag{3.15}$$

where the asterisk(*) denotes complex conjugation. If we express (3.14) as the inner product of the constrained weight vector $\underline{c}$ and the constraint vector $\underline{E}$ as

$$\langle \underline{c}, \underline{E} \rangle = 0, \tag{3.16}$$

then we recognize that the constraint vector $\underline{E}$ is orthogonal to the constrained excitation weight vector $\underline{c}$. The mathematical operation of the inner products of (3.16) for column vectors is defined as

$$\langle \underline{c}, \underline{E} \rangle = \underline{c}\underline{E}^H, \tag{3.17}$$

where H denotes the Hermitian transpose.

3.2 Solution

Utilizing the orthogonality between the constraint vector and the constrained excitation weight vector, the pattern approximation problem can now be solved using the well known least squares approximation method.

3.2.1 Least Squares Approximation

The objective is to approximate the quiescent weight vector $\underline{q}$ with a constrained weight vector $\underline{c}$ while minimizing the error vector. Referring to (3.12), minimizing ϵ is similar to minimizing the error vector, given by

$$\underline{e} = \underline{q} - \underline{c}. \tag{3.18}$$

Using basic algebra, the vector that minimizes the least squares error between $\underline{q}$ and $\underline{c}$ is the one that is orthogonal to $\underline{c}$.

In view of (3.16), we see that the constraint vector $\underline{E}$ is orthogonal to the constrained weight vector $\underline{c}$, thus the error vector in question is made up of a linear combination of the constraint vectors given in (3.15),

$$\underline{e} = \sum_{n=1}^{L} \beta_n \underline{E}_n, \tag{3.19}$$

where each β_n is a scaling factor and $L = N_1 + N_1 N_2$ is the total number of constraint vectors as described in (3.13) and (3.15) (there is one constraint vector for each constraint imposed). Substituting (3.19) into (3.18) and rearranging terms the constrained weight vector that gives us our least mean squared error pattern approximation subject to Multiple Null or Derivative Constraints is

$$\underline{c} = \underline{q} - \sum_{n=1}^{L} \beta_n \underline{E}_n. \tag{3.20}$$

The least mean squared solution has a nice interpretation which is apparent when we apply the linear relationship between a weight vector and its corresponding pattern shape to (3.20). In doing so, we see that the constrained pattern shown in (3.21) is the quiescent pattern minus a linear combination of the cancellation patterns,

$$W_c(k_x) = W_q(k_x) - \sum_{n=1}^{L} \beta_n W_{xn}(k_x), \tag{3.21}$$

where each W_{xn} is a cancellation pattern. The shape of the cancellation pattern is similar to the quiescent pattern. However, it is centered at the prescribed null location and scaled by β_n to match the amplitude of the quiescent pattern at the null location. This technique is similar to the one used in Applebaum's [3] adaptive algorithm for interference suppression.

Using the constraint vector $\underline{E}$, the cancellation wavenumber response function is given by

$$W_x(k_x) = \sum_{n=-N/2}^{N/2} E_n e^{-jndk_x}, \tag{3.22}$$

where each E_n is the element of the constraint vector in (3.15).

The scaling vector $\underline{\beta}$ can solved via (3.16). Substituting (3.20) into (3.16) yields

$$\underline{\nu} = \Phi \underline{\beta}, \tag{3.23}$$

where $\underline{\nu}$, $\underline{\beta}$, and Φ are defined as

$$\underline{\nu} = \begin{bmatrix} \langle \underline{q}, \underline{E}_1 \rangle \\ \langle \underline{q}, \underline{E}_2 \rangle \\ \langle \underline{q}, \underline{E}_3 \rangle \\ \vdots \\ \vdots \\ \langle \underline{q}, \underline{E}_L \rangle \end{bmatrix}, \tag{3.24}$$

$$\Phi = \begin{bmatrix} \langle \underline{E}_1, \underline{E}_1 \rangle & \langle \underline{E}_2, \underline{E}_1 \rangle & \langle \underline{E}_3, \underline{E}_1 \rangle & \cdots\cdots & \langle \underline{E}_L, \underline{E}_1 \rangle \\ \langle \underline{E}_1, \underline{E}_2 \rangle & \langle \underline{E}_2, \underline{E}_2 \rangle & \langle \underline{E}_3, \underline{E}_2 \rangle & \cdots\cdots & \langle \underline{E}_L, \underline{E}_2 \rangle \\ \langle \underline{E}_1, \underline{E}_3 \rangle & \langle \underline{E}_2, \underline{E}_3 \rangle & \langle \underline{E}_3, \underline{E}_3 \rangle & \cdots\cdots & \langle \underline{E}_L, \underline{E}_3 \rangle \\ \vdots & \vdots & \vdots & \vdots & \vdots \\ \vdots & \vdots & \vdots & \vdots & \vdots \\ \langle \underline{E}_1, \underline{E}_L \rangle & \langle \underline{E}_2, \underline{E}_L \rangle & \langle \underline{E}_3, \underline{E}_L \rangle & \cdots\cdots & \langle \underline{E}_L, \underline{E}_L \rangle \end{bmatrix}, \tag{3.25}$$

and

$$\underline{\beta} = \begin{bmatrix} \beta_1 \\ \beta_2 \\ \beta_3 \\ \vdots \\ \vdots \\ \beta_L \end{bmatrix}. \tag{3.26}$$

Thus, the scaling vector $\underline{\beta}$ is obtained by solving for the system of equations in (3.23) as follows,

$$\underline{\beta} = \Phi^{-1}\underline{\nu}. \tag{3.27}$$

In solving for the scaling vector $\underline{\beta}$, Eq. (3.27), its accuracy depends on the condition number of Φ or equivalently, the orthogonality of the constraint vectors $\underline{E}$.

The matrix Φ becomes ill conditioned when its columns or equivalently, when the constraint vectors $\underline{E}$ are approaching linear dependence. The orthogonality of the constraint vectors is examined in the next chapter.

Chapter 4

Results

The effectiveness of the null performance technique using Multiple Null Constraints and Derivative Constraints are presented in this chapter.

4.1 Multiple Null Constraints

The constrained wavenumber response function is subjected to Multiple Null Constraints or *zero-order* constraint when we set $i = 0$ in (3.13). For a spacing of a half wavelength ($d = \lambda/2$) and after evaluating Eq. (3.22), the *zero-order* of the cancellation function centered at $k_{x\alpha}$ is given by

$$W_x(k_x|k_{x\alpha}) = (N+1)\frac{\text{sinc}\left(\frac{1}{4}(N+1)(k_x - k_{x\alpha})\lambda\right)}{\text{sinc}\left(\frac{1}{4}(k_x - k_{x\alpha})\lambda\right)}, \tag{4.1}$$

where the function sinc(x) $= \frac{\sin(x)}{x}$.

Similarly, for normalized uniform weighting ($q_n = \frac{1}{(N+1)}$), the quiescent function simplifies to

$$W_q(k_x) = \frac{\text{sinc}\left(\frac{1}{4}(N+1)k_x\lambda\right)}{\text{sinc}\left(\frac{1}{4}k_x\lambda\right)}. \tag{4.2}$$

Using the previous two results and (3.21), the constrained function subjected to L single nulls is given by

$$W_c(k_x) = \frac{\text{sinc}\left(\frac{1}{4}(N+1)k_x\lambda\right)}{\text{sinc}\left(\frac{1}{4}k_x\lambda\right)} - (N+1)\sum_{n=1}^{L}\beta_n \frac{\text{sinc}\left(\frac{1}{4}(N+1)(k_x - k_{xn})\lambda\right)}{\text{sinc}\left(\frac{1}{4}(k_x - k_{xn})\lambda\right)}. \quad (4.3)$$

A plot for three arbitrarily chosen nulls imposed at the normalized spatial wavenumber $\frac{k_x\lambda}{\pi} = (0.95, 1.0, 1.05)$ is shown in Figure 4-1. Approximately, an average of 27 dB of sidelobe reduction is achieved across the null band. The sidelobe reduction Q is defined as the ratio of the maximum magnitude squared of the quiescent pattern to the maximum magnitude squared of the constrained pattern within the null band denoted by Δk_x. The expression for the sidelobe reduction ratio Q is given by

$$Q = \frac{\max\limits_{k_x \in \Delta k_x} |W_q(k_x)|^2}{\max\limits_{k_x \in \Delta k_x} |W_c(k_x)|^2}. \quad (4.4)$$

In the example shown in Fig. 4-1, the normalized null band is centered at $\frac{k_x\lambda}{\pi} = 1.0$ with a bandwidth of $\frac{\Delta k_x\lambda}{\pi} = 0.1$. The null band is defined as the sector that spans from the leftmost null to the rightmost null. For example, the normalized null band shown in Fig. 4-1 is from 0.95 to 1.05. Throughout this thesis and for Multiple Null Constraints only, the nulls are evenly separated over the null band with one null placed at each end of the null sector.

The price paid for the sidelobe reduction is the loss in the look direction gain or amplitude response and the change in the shape of the beampattern between the constrained and the quiescent cases. However, the look direction gain loss and the change in the pattern have been minimized in the least mean squared sense. The look direction gain loss GL_{look} is defined as the ratio of the magnitude response squared in the look direction of the quiescent pattern W_q and the constrained pattern W_c and is expressed as

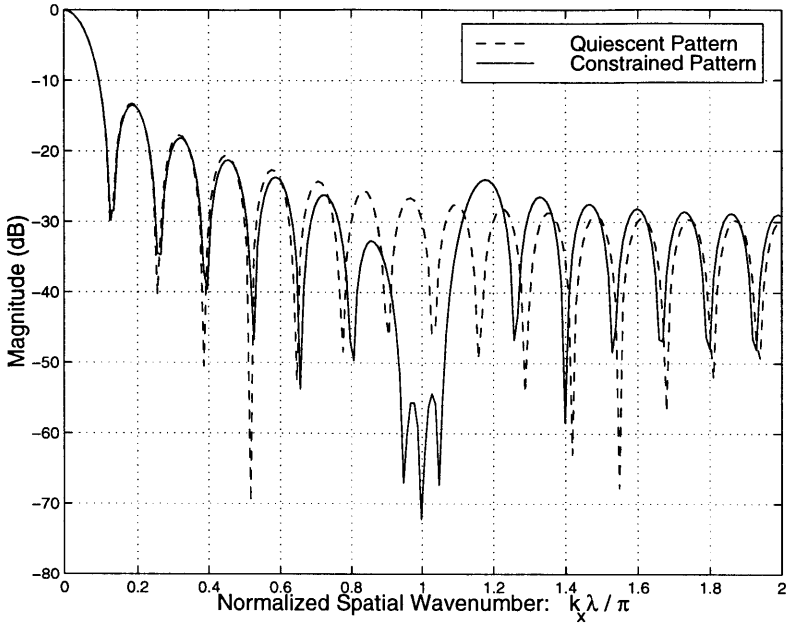

Figure 4-1: Multiple Null Constraints: Three single nulls imposed at $\frac{k_x\lambda}{\pi} = (0.95, 1.0, 1.05)$. Sidelobe reduction = 27dB, Look Direction Gain Loss = 0.06dB. Thirty-One element array with $d = \frac{\lambda}{2}$.

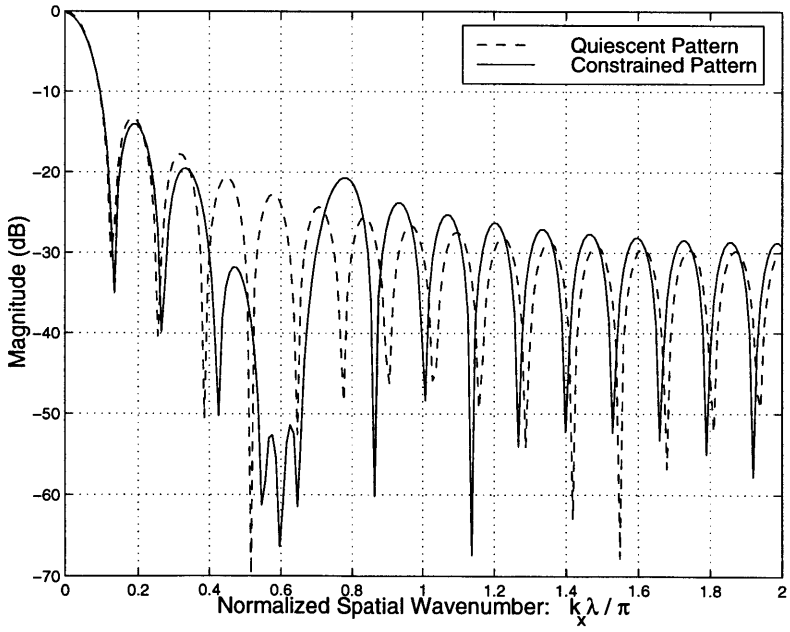

Figure 4-2: Multiple Null Constraints: Three single nulls imposed at $\frac{k_x\lambda}{\pi} = (0.55, 0.6, 0.65)$. Sidelobe reduction = 28dB, Look Direction Gain Loss = 0.18dB. Thirty-One element array with $d = \frac{\lambda}{2}$.

$$GL_{look} = \frac{|W_q(k_{x_{look}})|^2}{|W_c(k_{x_{look}})|^2}. \tag{4.5}$$

The look direction is at broadside for the case shown in Fig. 4-1.

The result shown in Fig. 4-1 incurs a 0.06 dB of look direction gain loss and the changes in the pattern are quite small in the directions away from the null band. In general, the effect of look direction gain loss is small (less than 1 dB) when the null's center is away from the mainlobe.

For a given number of imposed nulls and null bandwidth, the amount of sidelobe reduction achieved is independent of the level of the sidelobe to be reduced. This finding is illustrated in Figures 4-1 and 4-2. As shown in Fig. 4-2, the amount sidelobe reduction is approximately 28 dB. This result is similar to the 27 dB we obtain when the center of the null band is at 1.0, Fig. 4-1. Thus, it appears that amount of of sidelobe reduction achieved is independent of the amplitude of the sidelobe to be suppressed. For both cases, the number of imposed nulls used is three and the normalized null bandwidth is $\frac{\Delta k_x \lambda}{\pi} = 0.1$. The normalized null centers for Figures 4-1 and 4-2 are at 1.0 and 0.6, respectively. The difference in the location of the null centers implies a difference in the sidelobe level to be reduced in each case.

The independence of the sidelobe level to be reduced and the achieved sidelobe reduction is consistent with our analysis since the nulling technique was derived for any arbitrary quiescent pattern. The null performance should not vary for different wavenumbers when the number of constraints imposed and the null width remain fixed. This result is used in obtaining the overall null performance curves in a later section.

Another characteristic of the Multiple Nulling technique is that the level of sidelobe reduction increases as the number of imposed nulls increases for a fixed null bandwidth. This is illustrated in Figure 4-3. The result shown in Fig. 4-3 is for the case of four nulls evenly spaced over the normalized null band of [0.95, 1.05]. Note that this is the same null band as in Fig. 4-1. An average of 53 dB of sidelobe reduction is achieved over the null band. This is about a 26 dB increase in the

null performance as compared to the performance obtained when three nulls are used instead of four.

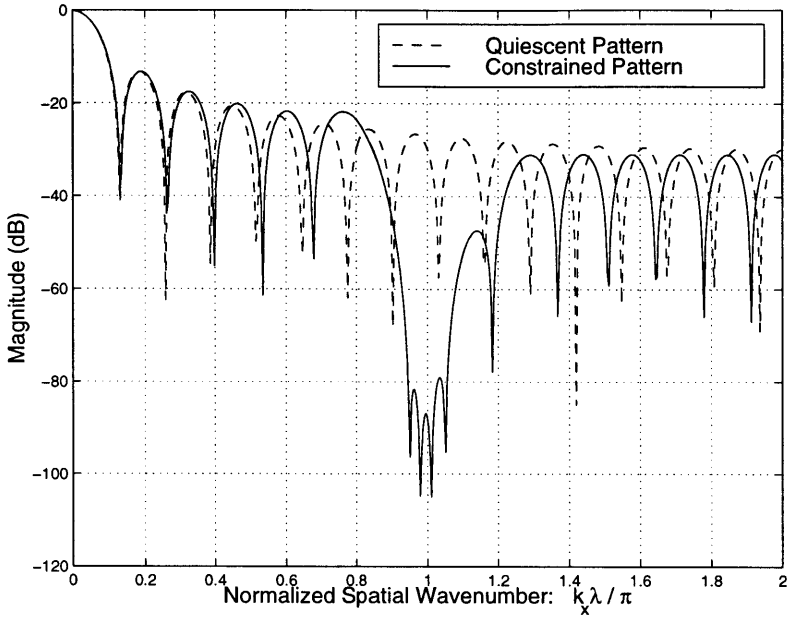

Figure 4-3: Multiple Null Constraints: Four single nulls evenly spanned over [0.95,1.05]. Sidelobe reduction = 53dB, Look Direction Gain Loss = 0.15dB. Thirty-One element array with $d = \frac{\lambda}{2}$.

Two performance metrics of a Multiple Null Constraints system are affected by the separation between each null: (i) the level of sidelobe reduction and (ii) the computational difficulty due to matrix ill conditioning. For the first case, the sidelobe reduction level increases as the null separation decreases. However, when the null separation is too small, the matrix Φ shown in (3.25) becomes ill conditioned since the columns are approaching linear dependence. Figures 4-4 and 4-5 show the plots of the condition number as a function of null separation for the case of two and three imposed nulls, respectively. We can see from both figures that the condition number is a function of the null separation and the number of imposed nulls. It is inversely related to the null separation and it increases with the number of imposed nulls. The inversion of the matrix becomes difficult when the condition number is large.

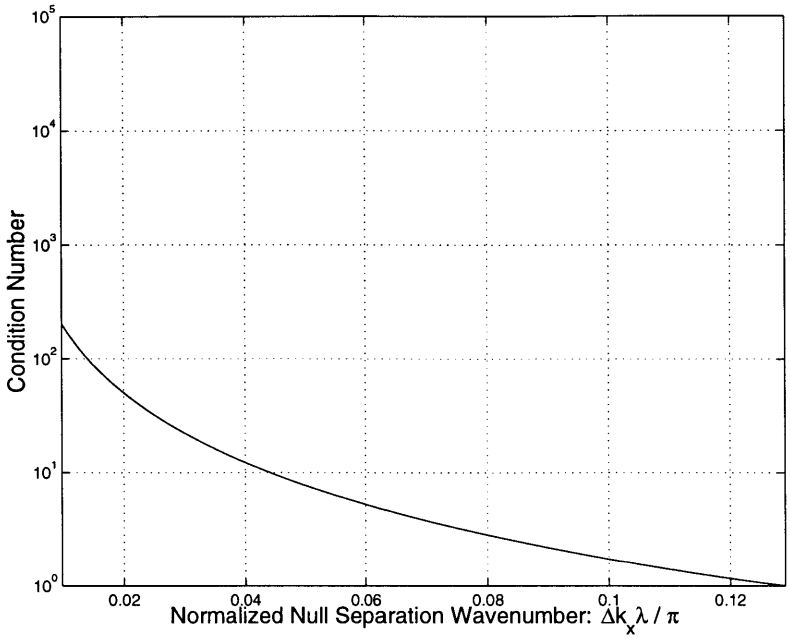

Figure 4-4: Multiple Null Constraints: Condition Number Vs. Null Separation for Two imposed Nulls.

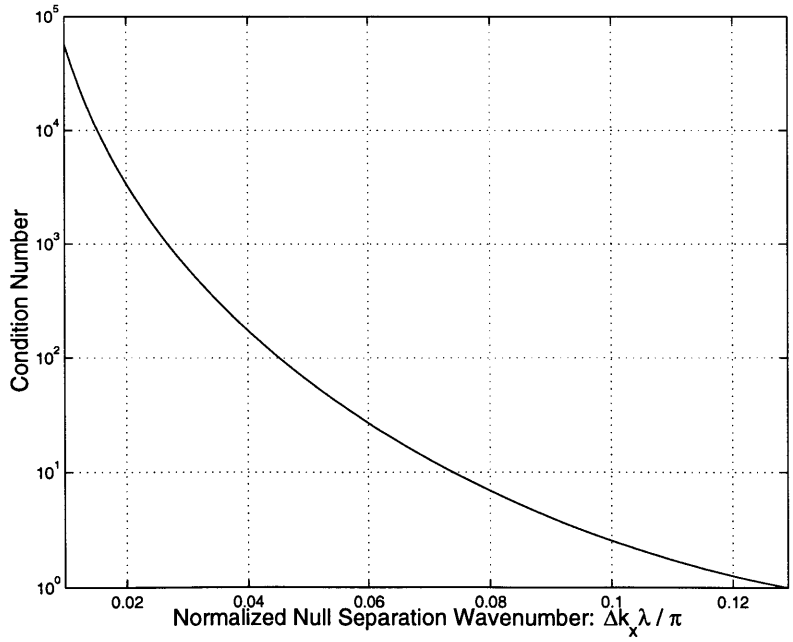

Figure 4-5: Multiple Null Constraints: Condition Number Vs. Null Separation for Three imposed Nulls.

4.1.1 Multiple Null Constraints Performance Summary

The null performance characteristics of the Multiple Null Constraints technique are:

1. The amount of sidelobe reduction achieved is independent of the sidelobe level to be reduced for a given number of imposed nulls and null bandwidth. That is, it requires as many constraints to reduce a sidelobe level from -10 dB to -20 dB as it does from -40 dB to -50 dB.
2. The sidelobe reduction level increases with the number imposed nulls for a given null bandwidth.
3. The sidelobe reduction increases as the separation between each null or the null bandwidth decreases. However, when the null separation is too small, the columns of the matrix Φ in (3.25) become linearly dependent and give rise to a large condition number. A large condition number causes difficulty in matrix inversion.
4. The loss in the look direction gain or amplitude response is quite small (i.e. less than 1 dB) when the null's center is away from the mainlobe. Also, the changes in the pattern occurs mostly in the vicinity of the null band.

The above performance characteristics will be compared to that of the Derivative Constraints technique in the next section.

4.2 Derivative Constraints

In this section we will present the results for two types of Derivative Constraints and they are *Hard* and *Soft* Constraints. We called it *Hard* Constraints because the derivative is constrained to zero at the null location as shown in Eq. (3.13). Similarly, *Soft* Constraints is when we relax this condition and instead we impose a non-zero derivative gain at the null location or by constraining the derivative to a small value δ. The results are shown in the next two sections.

4.2.1 Hard Constraints

The constrained wavenumber response function is subjected to Derivative Constraints when $i \geq 1$ in (3.13). In this method, we are imposing a zero-order pattern null together with higher order derivative nulls at the null location. Substituting the i^{th} order constraint of vector $\underline{E}$ shown in (3.15) into (3.22), the i^{th} order constraint of the cancellation function centered at $k_{x\alpha}$ is given by

$$W_g^{(i)}(k_x) = \sum_{n=-N/2}^{N/2} (-jnd)^i e^{-jnd(k_x - k_{x\alpha})}. \tag{4.6}$$

The i^{th} order constraint of the cancellation function can be simplified by recognizing that it is the i^{th} order derivative of the *zero-order* cancellation function,

$$W_g^{(i)}(k_x) = \frac{\partial^i}{\partial k_x^i}(N+1)\frac{\text{sinc}\left(\frac{1}{4}(N+1)(k_x - k_{x\alpha})\lambda\right)}{\text{sinc}\left(\frac{1}{4}(k_x - k_{x\alpha})\lambda\right)}. \tag{4.7}$$

The constrained function for L+1 constraints or the L^{th} order derivative constraint imposed at a single null located at $k_{x\alpha}$ is given by

$$W_c(k_x) = \frac{\text{sinc}\left(\frac{1}{4}(N+1)k_x\lambda\right)}{\text{sinc}\left(\frac{1}{4}k_x\lambda\right)} - (N+1)\sum_{i=1}^{L}\beta_i\frac{\partial^i}{\partial k_x^i}\frac{\text{sinc}\left(\frac{1}{4}(N+1)(k_x-k_{x\alpha})\lambda\right)}{\text{sinc}\left(\frac{1}{4}(k_x-k_{x\alpha})\lambda\right)}. \quad (4.8)$$

For notational convenience, the constrained pattern with *zero-order*, *zero-* plus *first-order*, *zero-* plus *first-* plus *second-order* constraints are termed *zero*, *first*, and *second − order* constraints, respectively.

Beampattern plots for *zero*, *first* and *second-order* constraints are shown in Figures 4-6 - 4-8 and a combined plot is shown in Figure 4-9. The use of derivative constraints to broaden a null is well demonstrated in Fig. 4-9. As expected, both the null depth and width increase with the constraint order. This is because additional flatness has been imposed by constraining zero derivative response at the null location.

One noticeable feature of Derivative Constraints is its ability to achieve a large null depth at the center of the band. However, the price paid for this large null depth is a decrease in the null width.

As we will see later that the trade-off between null depth and width is the key performance factor when choosing between Multiple Null Constraints and Derivative Constraints techniques. Figures 4-10 and 4-11 illustrate this trade-off by plotting the constrained pattern for the two techniques using two and three constraints, respectively. In comparing the results, the sidelobe reduction obtained with Multiple Null Constraints is less significant than with Derivative Constraints but it covers a wider sector.

Further examination of Figs. 4-10 and 4-11 suggests that a better overall null performance is achieved with Derivative Constraints when two constraints are used. Multiple Null Constraints gives better performance when the number of constraints is greater than two.

Similarly to Multiple Null Constraints, Derivative Constraints is subjected to look direction gain loss and pattern changes. Nevertheless, the gain loss is quite small for both constraint techniques and the changes in the pattern occur mostly in the vicinity of the null band.

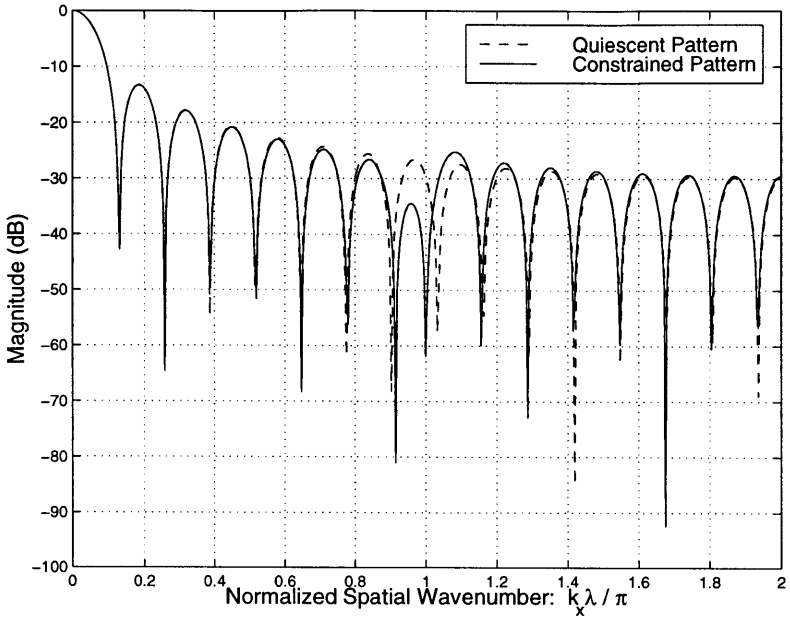

Figure 4-6: Derivative Constraints: *zero-order* constraint imposed at $\frac{k_x\lambda}{\pi} = 1.0$. Look Direction Gain Loss = 0.01dB. Thirty-One element array with $d = \frac{\lambda}{2}$.

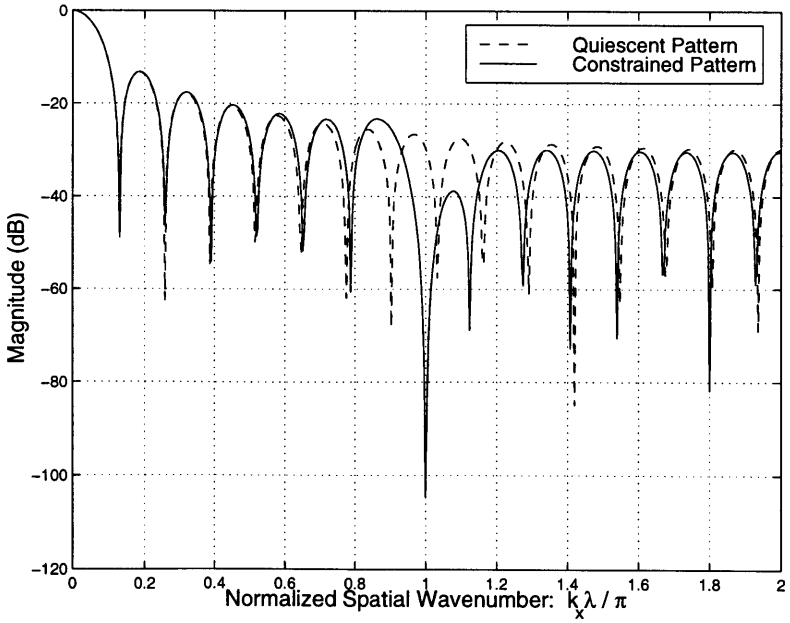

Figure 4-7: Derivative Constraints: *first-order* constraint imposed at $\frac{k_x\lambda}{\pi} = 1.0$. Look Direction Gain Loss = 0.03dB. Thirty-One element array with $d = \frac{\lambda}{2}$.

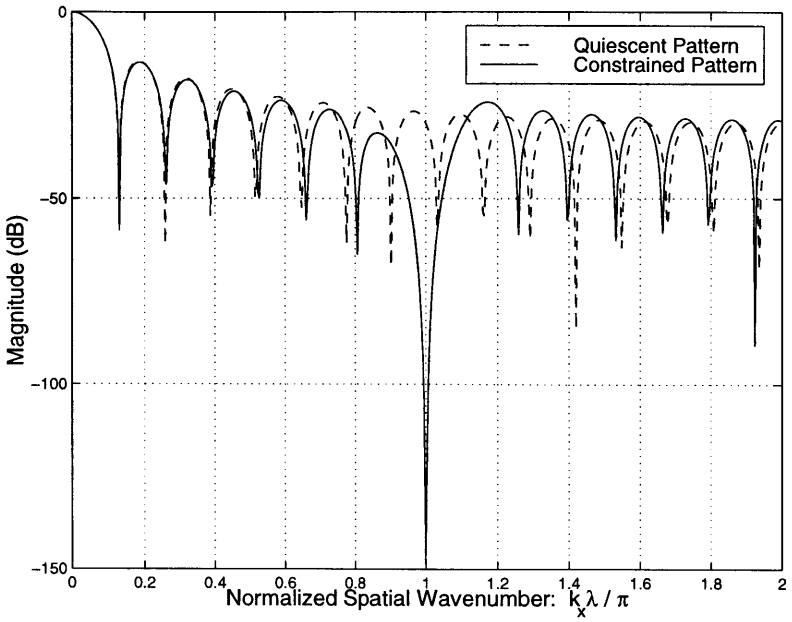

Figure 4-8: Derivative Constraints: *second-order* constraint imposed at $\frac{k_x\lambda}{\pi} = 1.0$. Look Direction Gain Loss = 0.07dB. Thirty-One element array with $d = \frac{\lambda}{2}$.

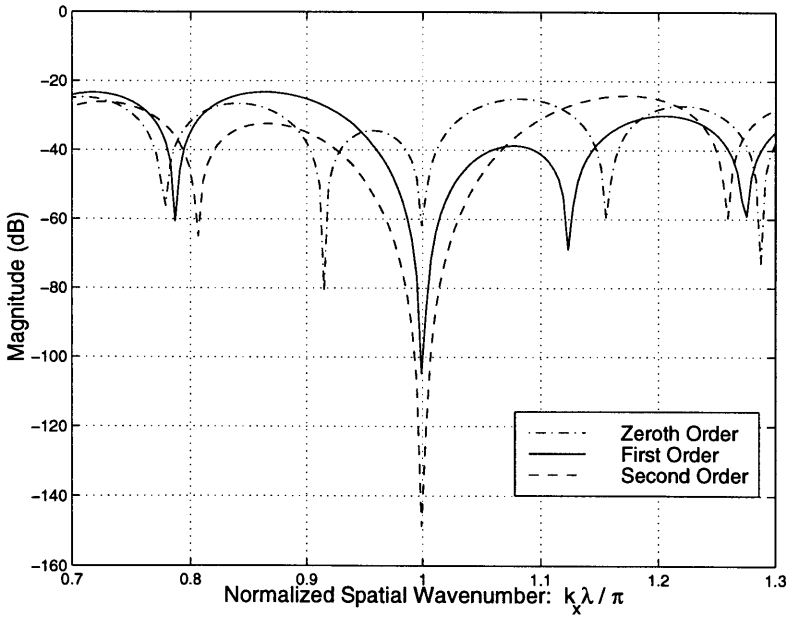

Figure 4-9: Derivative Constraints: The combined of *zero*, *first* and *second-order* constraints imposed at $\frac{k_x\lambda}{\pi} = 1.0$. Thirty-One element array with $d = \frac{\lambda}{2}$.

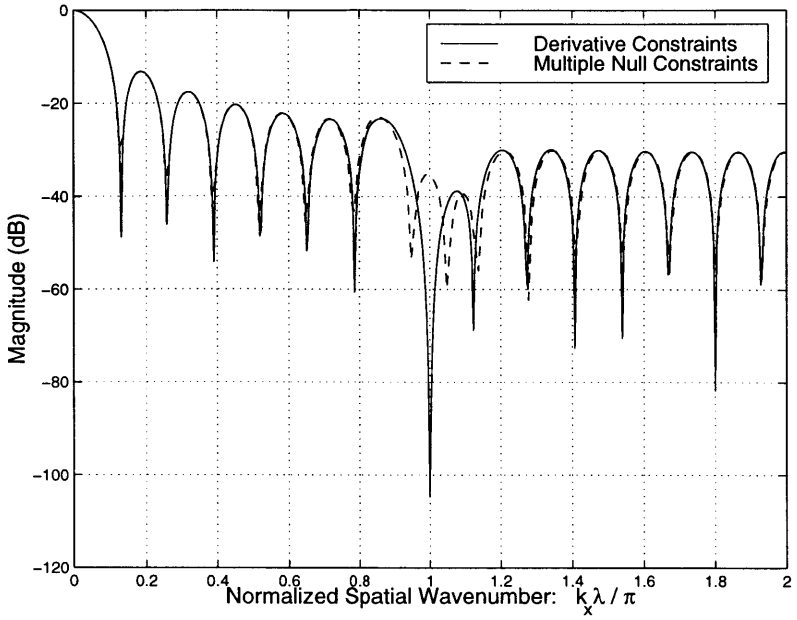

Figure 4-10: Comparison of Multiple Null and Derivative Constraints: Two constraints used (L=2) imposed at $\frac{k_x\lambda}{\pi} = 1.0$. The two null locations for Multiple Null Constraints are at $\frac{k_x\lambda}{\pi} = (0.95, 1.05)$. Thirty-One element array with $d = \frac{\lambda}{2}$.

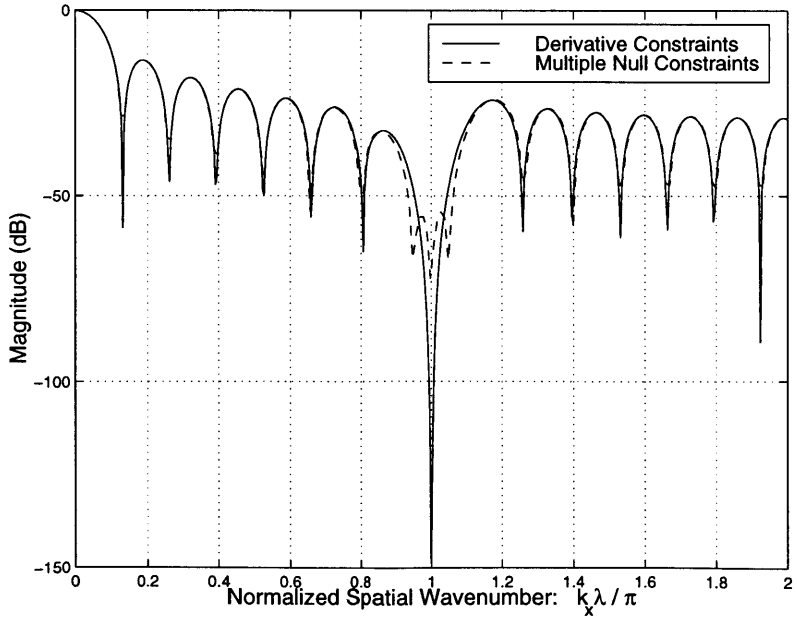

Figure 4-11: Comparison of Multiple Null and Derivative Constraints: Three constraints used (L=3) imposed at $\frac{k_x\lambda}{\pi} = 1.0$. The three null locations for Multiple Null Constraints are at $\frac{k_x\lambda}{\pi} = (0.95, 1.0, 1.05)$. Thirty-One element array with $d = \frac{\lambda}{2}$.

4.2.2 Soft Constraints

Due to the device performance limitation, any null depth beyond -70 dB is practically not realizable. As a result, the null performance obtain from the Hard Constraints method is practically not achievable, Fig. 4-9. Therefore, we now carry out the computations for the Soft Constraints method as an effort to reduce the null depth to a more practical range. In this method, we constrain equation (3.13) to a small value δ instead of to zero as for the Hard Constraints method.

Beampattern plots for the Soft Constraints method are shown in Figure 4-12 for three values of δ, -40dB, -60dB and -80dB. As expected the result of the Soft Constraints method approaches to that of the Hard Constraints method as $\delta \rightarrow 0$. Therefore by varying the constraining value δ, the null depth can be reduced to a desired operating value.

Two performance factors of a Derivative Constraints system are affected by imposing Soft Constraints on the null. First, the sidelobe reduction ratio Q, Eq. (4.4), decreases as a result of a decreased in the null depth. Second, the array white noise gain is expected to be less with the Soft Constraints method than with the Hard Constraints method. This will be apparent in the next section where we analyze for the array white noise gain of a beamformer.

4.3 Array White Noise Gain

The third performance metric use in comparing the performance between the two nulling techniques is the improvement in the signal-to-noise ratio or the array gain. As described by Cox et al. [6], the array gain is given by

$$G = \frac{\underline{w}^* \underline{s}}{\underline{w}^* R \underline{w}}, \tag{4.9}$$

where $\underline{w}$ is the array weighting vector, $\underline{s}$ is the signal vector and R is the noise cross-spectral matrix. The numerator of (4.9) is called the signal response, and the

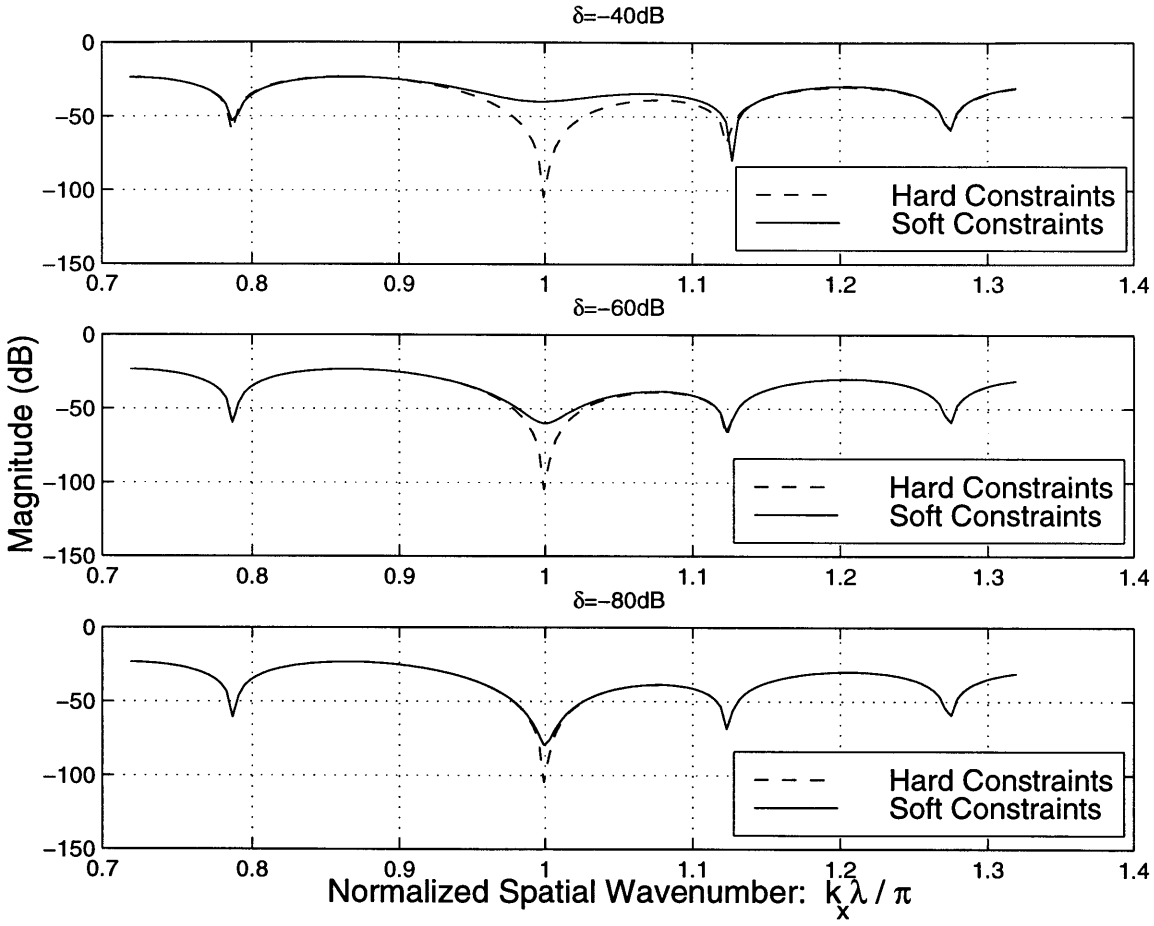

Figure 4-12: Beampattern plot for Soft and Hard Constraints methods. Normalized null center is at $\frac{k_x \lambda}{\pi} = 1.0$.

denominator is called the noise response. For the case of the noise is spatially white, the noise cross-spectral matrix R becomes the identity matrix and the array gain becomes what is called the *white noise gain.* We define the normalized white noise gain as

$$G_w = \frac{1}{\underline{w}^* \underline{w}}. \tag{4.10}$$

Thus, G_w is the array gain against spatially white noise and its reciprocal is a measure of sensitivity to noise. For a given nulling technique, higher value of white noise gain is desired thus making the pattern response less sensitive to additive noise.

A comparison plot of the normalized white noise gain for the Hard and Soft Derivative Constraints methods is shown in Figure 4-13 for $\delta = -40dB$. The plot shows that the Soft Constraints method exhibits a slightly less in the white noise gain than that of the Hard Constraints method. This is expected since the null depth has been reduced for the Soft Constraints method thus making it more sensitive to noise. However there is no difference in the white noise gain between each method for $\delta = -60dB$. This is shown in Figure 4-14 . Hence this allows us to use the Soft Constraint method without fear of making the beamformer more noise sensitive.

We have computed for the normalized array white noise gain for the Multiple Null Constraints and the Hard Derivative Constraints techniques for different values of L, the number of constraints imposed, and it is shown in Figure 4-15. The data shown in Figure 4-15 is the white noise gain of the constrained pattern G_{wc} normalized by the white noise gain of the quiescent pattern G_{wq}. Therefore, Figure 4-15 is the plot of the improvement in the array white noise gain due to pattern nulling constraints. As we can see that both nulling techniques achieve a similar level of improvement in the white noise gain. Therefore, the choice of which constraint technique to use becomes a matter of the user's preference between null depth and width.

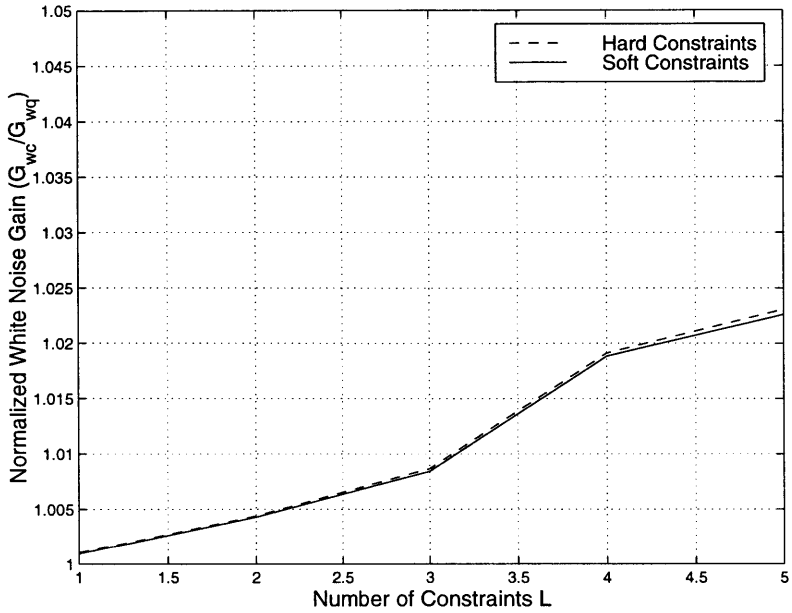

Figure 4-13: Comparison of Array White Noise Gain for Soft and Hard Constraints methods for $\delta = -40dB$.

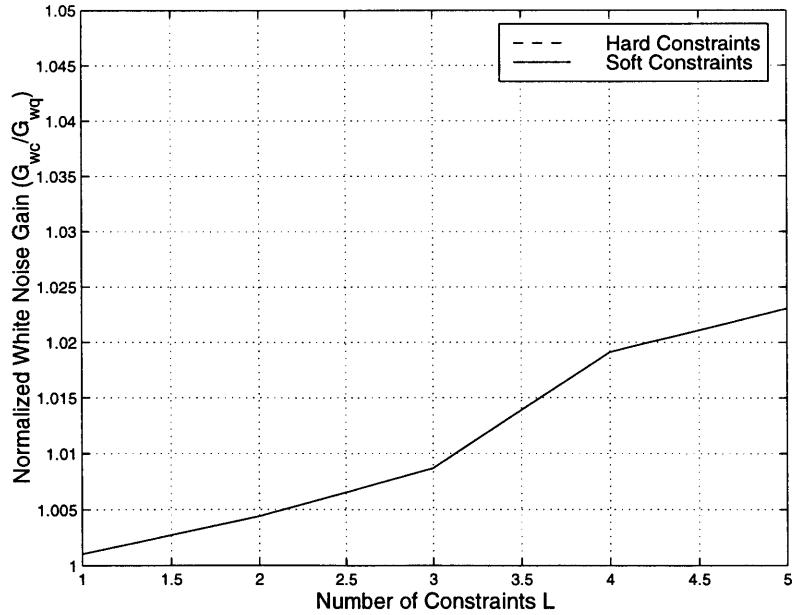

Figure 4-14: Comparison of Array White Noise Gain for Soft and Hard Constraints methods for $\delta = -60dB$.

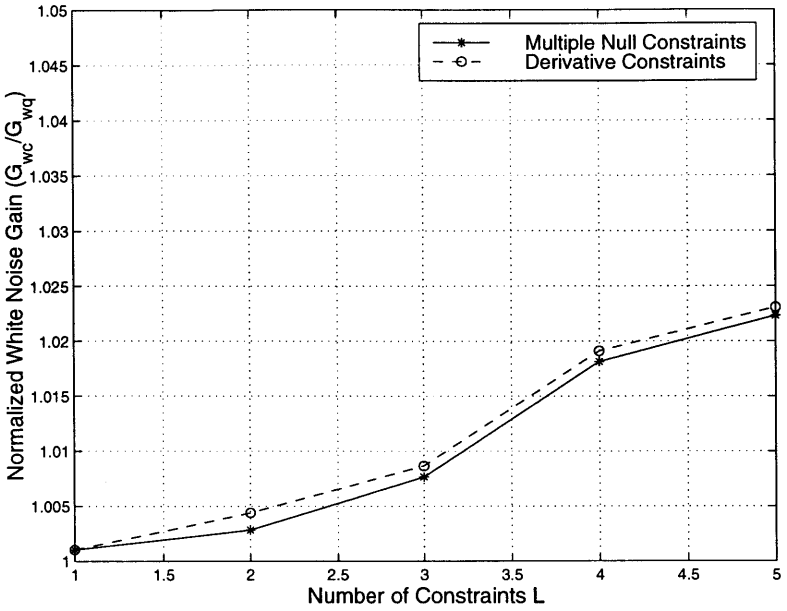

Figure 4-15: Array White Noise Gain G_w.

4.4 Overall Null Performance

Oftentimes in interference cancellation, one would like to know the relationship between the number of constraints and the achieved null width for a certain level of sidelobe reduction. As shown in Fig. 4-9, this relationship cannot be obtained directly with Derivative Constraints. Though the width of the null increases as the number of constraints is increased, quantifying the increase is difficult. In contrast, the relationship between the bandwidth and the number of nulls is well defined for Multiple Null Constraints since a null is imposed at each end of the band thus defining the null band.

In beamforming, it is generally efficient to minimize the number of constraints used for interference cancellation. Thus, we have computed general null performance curves for both techniques. These curves show the relationship between the level of sidelobe reduction achieved and the number of constraints used for a given null bandwidth.

The nulling performance curves for the Multiple Null Constraints and the Derivative Constraints techniques are shown in Figures 4-16 and 4-17 for different values of L, the number of imposed constraints. The performance curves are computed using

the average sidelobe reduction as given in (4.4) and is repeated here for completeness,

$$Q = \frac{\max\limits_{k_x \in \Delta k_x} |W_q(k_x)|^2}{\max\limits_{k_x \in \Delta k_x} |W_c(k_x)|^2}.$$

When computing for the reduction ratio for the Multiple Null Constraints technique, the nulls are evenly spanned out over the null band with one null placed at each end of the band. As for Derivative Constraints, the reduction ratio Q is computed as a function of the null band Δk_x (defined by the Multiple Null Constraints technique) for a given number of constraints L.

Examining the expression for Q, we see that it is a function of the location of the nulling band center. However, it has been shown in section 4.1 that the sidelobe reduction ratio is independent of the location of the band. It is a function of the bandwidth and the number of imposed constraints. The independence of the null location allows us to compute general performance curves for any location in the visible region of $\frac{k_x \lambda}{\pi} = [0, 2\pi]$.

Comparing the results shown in Figs. 4-16 and 4-17 and a comparison plot shown in Figure 4-18, we see that Multiple Null Constraints technique gives better average sidelobe cancellation than that of Derivative Constraints technique. This can be further justified by examining the comparison beampattern plot for both techniques shown in Figure 4-11. This plot clearly shows that over the null band defined by the Multiple Null Constraints technique, better average sidelobe cancellation is achieved with Multiple Null Constraints.

The performance curves we have presented thus far are for the case of an interelement spacing of one-half of a wavelength, $d = \lambda/2$. For half-wavelength spacing, the aliased space is equal to the propagation space. This is not the case for interelement spacing less than a half-wavelength or $d < \lambda/2$. In this case the propagation space is less than the aliased space. As a result, some of the sidelobes or noise energy which were in the propagation space (when $d = \lambda/2$) have now moved out into the aliased space. This is a concern because the mean squared error between the constrained

and quiescent patterns was minimized only over the propagating space. The added noise in the aliased space could affect the null performance since no error constraint was imposed in this space.

To examine this affect, we have computed a performance curve for the case of an interelement spacing of one-quarter of a wavelength $d = \lambda/4$. The result is compared to the case of half-wavelength spacing and is shown in Figure 4-19. As we can can see that the null performance is the same for both cases. Hence, the null performance curves we have presented thus far (for $d = \lambda/2$) are also applicable to other interelement spacing with $d < \lambda/2$.

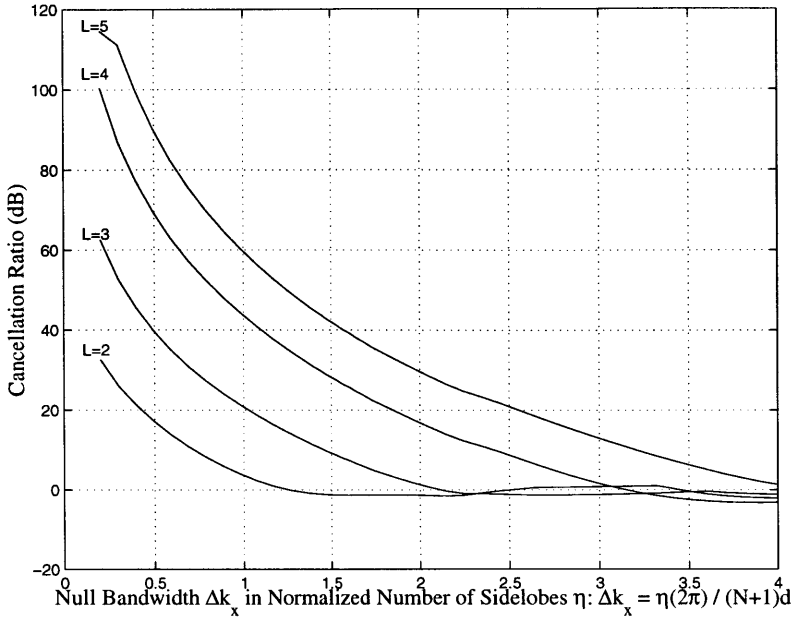

Figure 4-16: Multiple Null Constraints Nulling Performance Curves: L = number of imposed nulls.

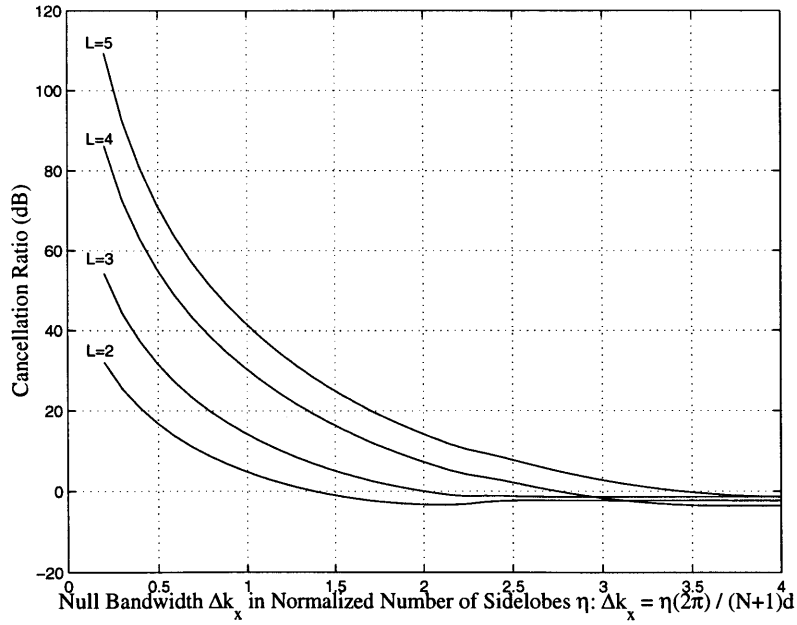

Figure 4-17: Derivative Constraints Nulling Performance Curves: L = number of imposed constraints.

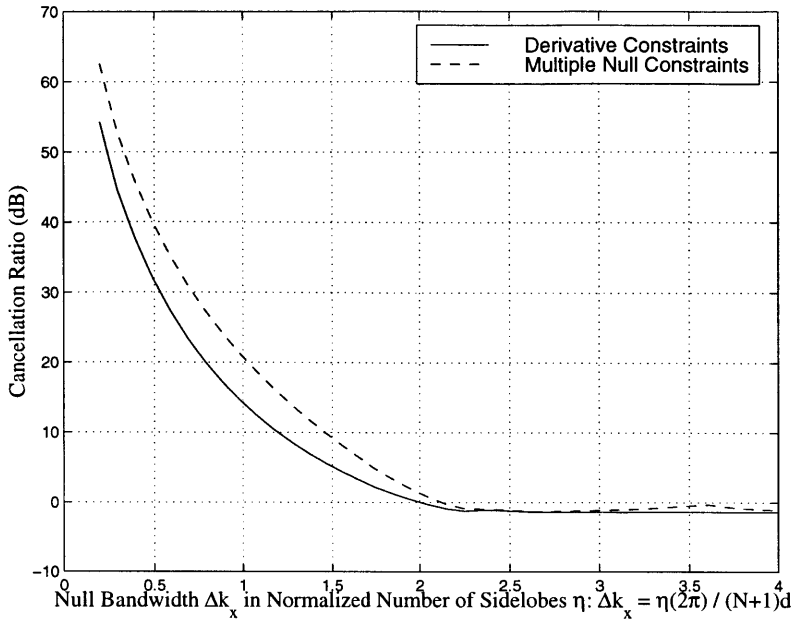

Figure 4-18: Comparison Nulling Performance Curves: Number of Constraints used L=3.

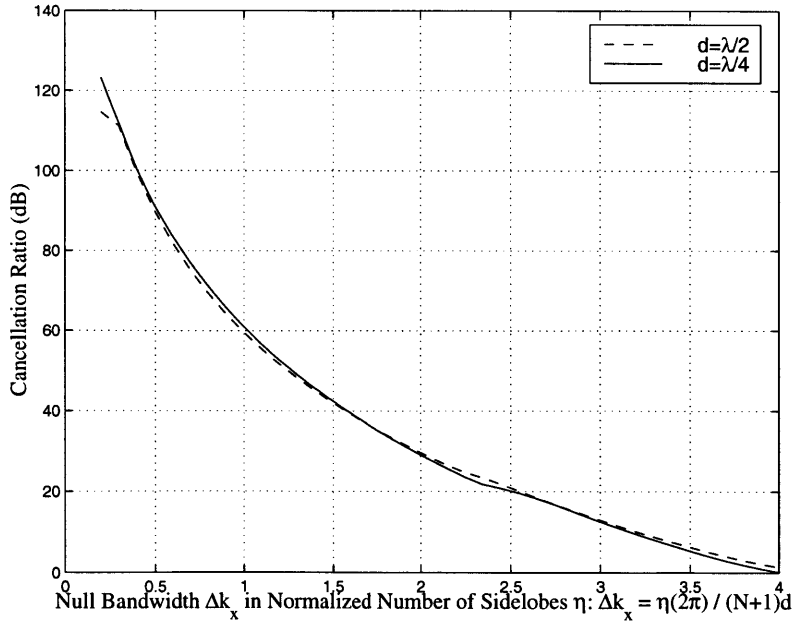

Figure 4-19: Nulling Performance Curves for interelement spacing of $d = \lambda/2$ and $d = \lambda/4$.

Chapter 5

Conclusion

In this thesis we have presented two beampattern nulling techniques, Multiple Null Constraints and Derivative Constraints. The resulting constrained pattern is a least mean squared approximation of the quiescent pattern subjected to pattern nulling requirements. Three performance merits, white noise gain, null width and null depth, were used to evaluate the effectiveness of each nulling technique. We have found that the improvement in the white noise gain is similar for both techniques. Thus, the choice of which constraint technique to use becomes a matter of the user's preference between null depth and width.

A major disadvantage of the Derivative Constraints technique is the indirect relationship between the number of constraints imposed and the resulting null bandwidth. This is not the case for Multiple Null Constraints in which the null bandwidth is the sector between the leftmost and rightmost nulls.

For a given number of constraints, the method of Derivative Constraints gives better depth but over a smaller sector than Multiple Null Constraints. The latter technique yields less depth but over a wider sector. Better overall performance is achieved with Derivative Constraints when the number of constraints used is two.

As we have seen earlier that the null depth obtain from the *Hard* Derivative Constraints method is quite large. However, any null depth beyond -70 dB is practically not realizable due to the device performance limitation. As a result, a *Soft* Constraints method was considered. The data have shown that the result of the Soft Constraints

method approaches to that of the Hard Constraints method as the constraining value $\delta \rightarrow 0$. Thus, by varying the constraining value δ, the null depth can be reduced to a more practical range.

General sidelobe nulling performance curves were computed for both techniques. The performance curves show the relationship between the average level of sidelobe reduction achieved over some nulling bandwidth for a given number of constraints. After comparing the performance curves we have concluded that Multiple Null Constraints technique gives better average sidelobe reduction ratio than that of Derivative Constraints technique.

In conclusion, for wide-band interference cancellation applications, multiple nulling is more effective than derivative nulling. Conversely, when the interfering source is narrow-band or directional, derivative nulling is more effective than multiple nulling due its ability to achieve a large null depth at the interfering direction.

Bibliography

[1] Davies, D. E. N.: 'Independent angular steering of each zero of the directional pattern for a linear array', IEEE Transactions on Antenna and Propagation, Vol. AP-15, 1967, pp. 296-298.

[2] Drane, C., and McIlvenna, J.:'Gain Maximization and Controlled Null Placement Simultaneously Achieved in Aerial Array Patterns, Radio and Electronic Engineer, Vol. 39, No. 1, Jan. 1970, pp. 49-56.

[3] Applebaum, S.:'Adaptive Arrays', IEEE Transactions on Antenna and Propagation, Vol. AP-24, 1976, pp. 585-598.

[4] Er, M., and Cantoni, A.:'Derivative Constraints for Broad-Band Element Space Antenna Array Processors' IEEE Transactions on ASSP, Vol. ASSP-31, No. 6, Dec. 1983, pp. 1378-1393.

[5] Applebaum, S., and Chapman, D.:'Adaptive Arrays with Main Beam Constraints', IEEE Transactions on Antenna and Propagation, Vol. AP-24, No. 5, 1976, pp. 650-662.

[6] Cox, H., Zeskind, R., and Owen, M. :'Robust Adaptive Beamforming', IEEE Transactions on Acoustics, Speech, and Signal Processing, Vol. ASSP-35, No. 10, 1987, pp. 1365-1375.